Check for updates

Volume 18 | Number 1 | 7 January 2016 | Pages 1–636

PCCP

Physical Chemistry Chemical Physics
www.rsc.org/pccp

ISSN 1463-9076

ROYAL SOCIETY OF CHEMISTRY

PERSPECTIVE
Darya Radziuk and Helmuth Möhwald
Ultrasonically treated liquid interfaces for progress in clearing and separation processes

175 YEARS

ROYAL SOCIETY OF CHEMISTRY

rsc.li/pccp

Alamethicin self-assembling in lipid membranes: concentration dependence from pulsed EPR of spin labels

Victoria N. Syryamina,[a,b] Marta De Zotti,[c] Claudio Toniolo,[c,d] Fernando Formaggio,[c,d] and Sergei A. Dzuba[a,b,]*

[a]Institute of Chemical Kinetics and Combustion, RAS, Novosibirsk 630090, Russian Federation

[b]Novosibirsk State University, Novosibirsk 630090, Russian Federation

[c]Department of Chemical Sciences, University of Padova, 35131 Padova, Italy

[d]Institute of Biomolecular Chemistry, Padova Unit, CNR, 35131 Padova, Italy

†Electronic supplementary information (ESI) available

*Correspondence to: dzuba@kinetics.nsc.ru

Abstract

The antimicrobial action of the peptide antibiotic alamethicin (Alm) is commonly related to peptide self-assembling resulting in the formation of voltage-dependent channels in the bacterial membranes, which induce ion permeation. To obtain a deeper insight into the mechanism of channel formation, it is useful to know the dependence of self-assembling from peptide concentration. To this aim, we studied Alm F50/5 spin-labeled analogs in a model 1-palmitoyl-2-oleoyl-*sn*-glycero-3-phosphocholine (POPC) membrane, for peptide-to-lipid (P/L) ratios varying between 1/1500 and 1/100. Pulsed electron-electron double resonance (PELDOR) spectroscopy reveals that even at the lowest concentration investigated the Alm molecules assemble into dimers. Moreover, under these conditions electron spin echo envelope modulation (ESEEM) spectroscopy of D_2O-hydrated membranes shows a peptide abrupt change from the in-plane to the trans-membrane orientation. Therefore, we hypothesize that dimer formation and peptide reorientation are concurrent processes and represent the initial step of peptide self-assembling. By increasing peptide concentration, higher oligomers are formed. A simple kinetic model of equilibrium among monomers, dimmers, and pentamers allows for satisfactorily describing the experimental PELDOR data. The inter-label distances in the oligomers obtained from PELDOR experiments become better resolved within creasing P/L ratio, thus suggesting that the supramolecular organization of the higher-order oligomers becomes more defined.

1. Introduction

Antimicrobial peptides (AMP) belonging to the naturally occurring peptaibiotic family are known for their ability to modify the permeability of biological membranes.[1-4] Peptaibiotics are characterized by the presence in the sequence of a non-coded α-amino acid, α-aminoisobutyric acid (Aib), an N-terminal acyl moiety, most often an acetyl (Ac), and a C-terminal 1,2-amino alcohol. Alamethicin (Alm), isolated from the fungus *Trichoderma viride*, is a hydrophobic 19-amino acid peptaibiotic. It is one of the most extensively studied antimicrobial peptides.[5] In membranes Alm adopts a mixed $\alpha/3_{10}$-helix structure, thus spanning a length of about 2.6-3.0 nm.[6-8]

The antimicrobial action of Alm is commonly related to the formation of stable channels (pores) with well-defined conductance levels. At low P/L ratio, the peptide molecules are randomly distributed in the membrane but preferably parallel to itssurface.[9] When the P/L ratio increases up to a threshold value, P/L*, peptides self-assemble to form channels. The polar face of the peptide helix lays in the inner side of the channels (barrel-stave and worm-hole pores).[9] Channel formation may be accompanied by peptide helix tilting or transition to the fully transmembrane orientation. Depending on the degree of peptide oligomerization, the inner size of the pores varies, allowing to transport small ions, water or even large polar molecules.

The mechanism of channel formation by AMP depends on hydrophobic matching conditions, peptide concentration in membrane, ion gradient, and hydration level.[5,10,11] Alm molecules are large enough to span almost all membranes (up to the thickest membranes with 2.6 nm hydrophobic length). Therefore, they may form pores in the absence of transmembrane potential,[12] or be monomeric even at high P/L ratio.[13]

Alm molecules in model biological membranes at a P/L ratio above ~ 1/250 were found to be in the transmembrane self-assembled state.[7,14,15] Molecular dynamics (MD) simulations showed that the stable state for Alm in membranes is an aggregate of at least five molecules.[16] A detailed model of Alm ion channel supramolecular structure was suggested from pulsed EPR of spin labeled analogs in a zwitter-ionic egg L-α-phosphatidylcholine (ePC) model membrane:[7] for a P/L ratio varying between 1/200 and 1/70, Alm forms a pyramid-like tetramer with parallel helices in which two rigidly oriented peptides and other two peptides may be tilted ("pen-knife" model). Another channel structure was proposed by NMR data in the zwitter-ionic POPC membrane:[8] for a P/L ratio =1/30, Alm is assembled into dimers that evolve to pentamers when the P/L ratio increases to 1/15. Also, oligomers of higher order were proposed, including hexamers and octamers.[16-19]

To elucidate the molecular mechanisms of oligomerization and accompanying channel formation, it would be helpful to throw light on the sequential steps of peptide self-association, which may occur as the P/L ratio increases. In this work, we studied the self-association of spin-labeled Alm F50/5 analogs, for the P/L ratio ranging from 1/1500 to 1/100, by exploiting different techniques of electron paramagnetic resonance (EPR) spectroscopy: conventional continuous wave (CW) EPR, pulsed electron-electron double resonance (PELDOR),[20-23] and (electron spin echo envelope modulation) ESEEM.[24-26] PELDOR allows one to obtain the number of spin-labeled molecules in an oligomer and to find the inter-label distances in the range between 1.5 and 6-8 nm. ESEEM of D_2O-hydrated membranes provides information on the spin label localization within the membrane.

2. Pulse EPR data analysis

2.1 PELDOR

PELDOR spectroscopy is based on electron spin echo (ESE) technique which is a pulsed version of EPR. The PELDOR signal is the ESE signal observed at a detection frequency ω_A and influenced by application of an additional microwave pumping pulse acting at a different microwave frequency ω_B;[20-23] it is varying with a delay T of the pumping pulse. The PELDOR signal amplitude, $V(T)$, for spin labels arranged in clusters (oligomers), distributed in space, is given by the product of two factors:[21]

$$V(T) = V_{INTRA}(T)V_{INTER}(T) \qquad (1)$$

where $V_{INTRA}(T)$ is an intra-cluster contribution to dipolar interaction, $V_{INTER}(T)$ is an inter cluster contribution (usually its dependence on T is close to the exponential function). However, its deviation from an exponential dependence may become noticeable, for instance, in the case of reduced dimensionality.[21] Therefore, the logarithm of $V_{INTER}(T)$ is usually approximated by a polynomial.

Experimentally, $V_{INTRA}(T)$ and $V_{INTER}(T)$ manifest themselves as short-time and long-time signal decays. For spin labels assembled in pairs, spins A and B,[21]

$$V_{INTRA}(T) = 1 - p_B(1 - f(T)), \qquad (2)$$

where, for spin labels distributed by a distance r in the pairs with the probability density $P(r)$ (normalized as $\int_0^\infty P(r)dr = 1$), and randomly oriented in the angular space

$$f(T) = \int_0^\infty P(r)dr \int_0^\pi \sin\theta d\theta \cos\left(\frac{g^2 \mu_B^2}{\hbar r^3}(1 - 3\cos^2\theta)T\right) \qquad (3)$$

5

where g is the g-factor, μ_B is the Bohr magneton, and θ is the angle between the vector **r**

joining two spins and the external magnetic field.

Then, the dimensionless parameter p_B in Eq. (2) reflects the off-resonance effects of

the microwave excitation in the pair[21,27]

$$p_B = \frac{p_B^0}{1 - p_A^0}, \, p_{B(A)}^0 = \int_0^\infty \frac{\omega_1^2}{\omega_1^2 + (\omega - \omega_{B(A)})^2} \sin^2\left(\frac{\tau_{pulse}}{2}\sqrt{\omega_1^2 + 4\pi^2(\omega - \omega_{B(A)})^2}\right) g(\omega)d\omega \quad (4)$$

where $g(\omega)$ is the absorptive EPR lineshape, ω_1 is the pulse amplitude in angular frequency

units, τ_{pulse} is the pulse length, and n is the number of spins in an oligomer.

When analyzing the intra-pair dipolar interaction $V_{INTRA}(T)$, the parameter p_B is

excluded and the normalized V_{norm} function is employed:[28]

$$V_{norm}(T) = \frac{V_{INTRA}(T) - V_{INTRA}(\infty)}{1 - V_{INTRA}(\infty)} \quad (5)$$

For the clusters consisting of n molecules, in the absence of multi-spin interactions

(see below), instead of Eq. (2) one can write[21]

$$V_{INTRA}(T) = (1 - p_B(1 - f(T)))^{n-1} \quad (6)$$

The three-spin interactions may be neglected when the $(n-1)\,p_B$ parameter is small.[29] For

large values of this parameter, the contribution of multi-spin interactions (when $n > 2$) should

be considered.[29] In this case, the spectra analysis becomes complicated as the probability of

inversion of more than one spin in the cluster increases.[29,30]

From Eqs. (2) (3) and (5) it follows that the experimentally obtained $V_{norm}(T)$ function for pairs of spin labels corresponds to the $f(T)$ function. Therefore, one can find the distance distribution function $P(r)$ by solving the integral equation (3), which is a first-kind Fredholm integral equation. Since solving this equation is however an ill-posed problem, a regularization is needed. The most commonly used is the Tikhonov regularization which imposes restrictions on smoothness of the solution.[31] Regularization can also be done in other ways, *e.g.* by increasing the discretization length for the solution[32] or by approximating the solution by a sum of restricted number of Gaussians (multi-Gaussian fit).[33,34] Here, we use the multi-Gaussian fit employing a fully random Monte Carlo process in the frequency domain.[34] Note that in this approach the rate of convergence is rather high because of singularity in the core of the integral equation (3) when it is transferred to the frequency domain.

From Eq. (2) it follows that the analysis of the intramolecular PELDOR decay allows counting the number n of spin labeled molecules assembled in a cluster.[26,28-30,35] Indeed, at the infinite time limit $f(T) \rightarrow 0$, the asymptote

$$V_{INTRA}(\infty) = (1 - p_B)^{n-1} \tag{7}$$

can be directly used for this counting.

2.2. ESEEM

The three-pulse stimulated ESEEM is obtained for the pulse sequence $\pi/2-\tau-\pi/2-T-\pi/2-\tau-echo$, with the time delay T scanned. The ESEEM data analysis was described elsewhere.[24,25] Briefly, the original ESEEM signal, $E(T)$, is normalized to exclude the non-modulated part of the echo decay:

$$E_n(T) = \frac{E(T)}{<E(T)>} - 1 \tag{8}$$

Physical Chemistry Chemical Physics Accepted Manuscript

where $<E(T)>$ is a non-oscillating function which smoothly approximates the original $E(T)$ time trace. Then, the ESEEM signal is transformed into the frequency domain:

$$F_C(f) = \int_{t_{min}}^{t_{max}} E_n(t)\exp(2\pi ift)dt \qquad (9)$$

where $t = \tau + T$, t_{min} and t_{max} are the lower and upper boundaries attained for the t variation in the experiment. For ^{2}H-induced ESEEM from remote nuclei, the frequency spectrum consists of a single narrow line located at the ^{2}H Larmor frequency (2.2 MHz at the X-band EPR). The influence of the missing data at $0 < t < t_{min}$ is reduced substantially by using the absolute-value spectra, $F(f) = |F_C(f)|$. Note that $F(f)$ (spectral density) has dimension of time and does not depend on the spectrometer parameters (amplification, time step, *etc*.).

3. Experimental

3.1. Sample preparation

The syntheses and characterizations of the two Alm F50/5 spin-labeled analogs, Alm1 and Alm16 (Scheme 1), investigated in this work were already reported.[36]

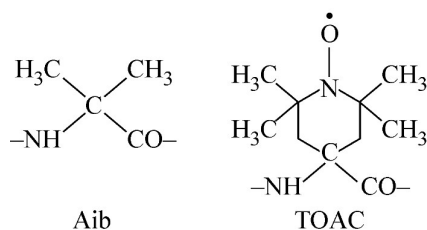
Scheme 1. Top: α-Amino acid sequences of the spin-labeled analogs of alamethicin F50/5. Bottom: Chemical structures of the α-amino acids Aib and TOAC

Ac-TOAC^1-Pro-Aib-Ala-Aib-Ala-Glu(OMe)-Aib-Val-Aib-Gly-Leu-Aib-Pro-Val-Aib^{16}-Aib-Glu(OMe)-Glu(OMe)-Phl (Alm1)

Ac-Aib^1-Pro-Aib-Ala-Aib-Ala-Glu(OMe)-Aib-Val-Aib-Gly-Leu-Aib-Pro-Val-TOAC^{16}-Aib-Glu(OMe)-Glu(OMe)-Phl (Alm16)

Aib   TOAC

TOAC is 4-amino-1-oxyl-2,2,6,6-tetramethylpiperidine-4-carboxylic acid; OMe is methoxy; Phl is phenylalaninol.

It is worth noting that the amino acid substitution Gln→Glu(OMe) at the 7th, 18th, and 19th positions does not alter significantly the behavior of these analogs, as compared to the naturally produced alamethicin. In particular, it does influence neither the 3D structure[37] nor the pore stabilization.[12]

The lipid POPC was obtained from Avanti Polar Lipids (Birmingham, AL). Methanol, ethanol and chloroform were Ekros-Analytica (St. Petersburg, Russia) products. The deuterated 10 mM PBS buffer was prepared as aqueous 0.137 M NaCl and 0.0027 M KCl solutions, which provide pH = 7.0 (Biolot, St. Petersburg, Russia).

The lipids with Alm1 or Alm16 added at different P/L ratios between 1/1500 and 1/100 were dissolved in chloroform in an EPR glass tube of 5 mm diameter. The solvent was slowly removed by a nitrogen flow with subsequent storage for 4 h under vacuum (10^{-2} bar). Then, the dry peptide/lipid film at the tube walls was dispersed in buffer (the buffer weight amount was nearly the same as that for the film) by vortex mixing, with subsequent 5 cycles of rapid freezing-thawing. Following this protocol, large multilamellar vesicles (LMV) are expected to form.[38] The samples were stored at room temperature for 2 h and then rapidly frozen and stored in liquid nitrogen.

For calibration purposes, the lipid spin-labeled at the polar head, 1,2-dipalmitoyl-sn-glycero-3-phospho(tempo)choline (Tempo-PC) (Avanti Polar Lipids, Birmingham, AL), and

the stearic acid spin-labeled at the 5th carbon position, 5-Doxyl-stearic acid (5-DSA) (Sigma-Aldrich), were used in sample preparations at a molar ratio of 1/100 in exactly the same way as that described above for the spin-labeled peptides. Also for calibration purposes, the rigid biradical **BR** (its structure is shown in ESI†, Fig. 1S) dissolved in a glassy methanol/ethanol mixture (95/5 *v/v*) was used.

3.2 CW EPR

CW EPR spectra were obtained with an X-band Bruker E380 EPR spectrometer by using a dielectric Bruker ER 4118 X-MD-5 cavity and an Oxford Instruments CF-935 cryostat cooled down to 100 K by evaporating nitrogen gas. The modulation amplitude of 0.05 mT and modulation frequency of 100 kHz were used. The microwave power was set low enough to avoid EPR spectra saturation.

3.3 Pulsed EPR

The three-pulse PELDOR and ESEEM experiments were performed on an X-band Bruker ELEXSYS E580 EPR spectrometer using a split-ring Bruker ER 4118 X-MS-3 cavity and an Oxford Instruments CF–935 cryostat cooled down to 80 K.

In PELDOR experiments, the echo signal was detected with a two-pulse sequence $\pi/2_{(\nu A)}$-τ-$\pi_{(\nu A)}$-τ-$echo_{(\nu A)}$ applied at the microwave detection frequency ν_A and with an additional pumping pulse $\pi_{(\nu B)}$ applied at the pumping frequency ν_B. The pumping pulse initially preceded the first detection pulse by 188 ns and then it was scanned forward with a time step of 4 ns. The pumping and observation frequencies were set symmetrically around the center of the resonator dip. The pumping pulse frequency ν_B was set to excite the maximum of the echo-detected (ED) EPR spectra and the observation frequency ν_A was applied with an offset ν_A-ν_B=70 MHz. [In some experiments the reverse offset was used: ν_A

corresponded to the maximum of the ED EPR spectrum and the pumping frequency was 70 MHz higher (ν_A-ν_B=-70 MHz)] .The length of all pulses was set to 40 ns. The amplitudes of the echo-detecting $\pi/2$- and π-pulses varied independently to provide maximum echo signal. A two-step phase-cycling for pulses and detection was performed: (+,+,+),(-,+,-). The amplitude of the pumping π-pulse was adjusted to obtain a maximal echo inversion in the experiment with ν_A=ν_B and the pumping pulse preceding the echo-forming pulses. For experiments with the pumping pulse amplitude varying, the amplitude was decreased by an attenuator.

The time τ was chosen as 0.8 μs for samples with the P/L ratio< 1/100 and 0.5 μs for sample with the P/L ratio = 1/100. The distortion of the PELDOR signal on the pumping pulse passage through the detection pulse were eliminated as described previously.[39] Fourier transformation of the normalized $V_n(T)$ PELDOR time traces was performed with a Hemming apodization window of 0.8 μs. The multi-Gaussian Monte-Carlo simulation for the pair distance distribution function[34] was carried out using a home-made program written in the Pascal ABC software.

The three-pulse ESEEM experiments, *π/2-τ-π/2-T-π/2-τ-echo*, were performed at the maximum of the ED EPR spectra. The pulse length was 16 ns, τ was 204 ns, and the *T* interval was scanned from 348 ns to 10 μs, with a time step of 12 ns. The relaxation decay was fit in a *semi*logarithmic plot by a 6th-order polynomial. The modulus-Fourier transformation was carried out with a home-made MatLab program.

4. Results

4.1.Non-hydrated *vs.* hydrated samples

CW EPR and PELDOR data obtained for dry and hydrated peptide/lipid films (see 3.1 Sample preparation) were compared for Alm16 at the P/L ratio 1/400. The results are shown

in Fig.1. The CW EPR spectra (Fig. 1A) consist of well resolved lines typical for diluted immobilized nitroxide. Upon hydration some linewidth increase can be noticed. This effect may be related with an increase of the dipole-dipole interaction between unpaired spins which indicates peptide self-assembling in the membrane.
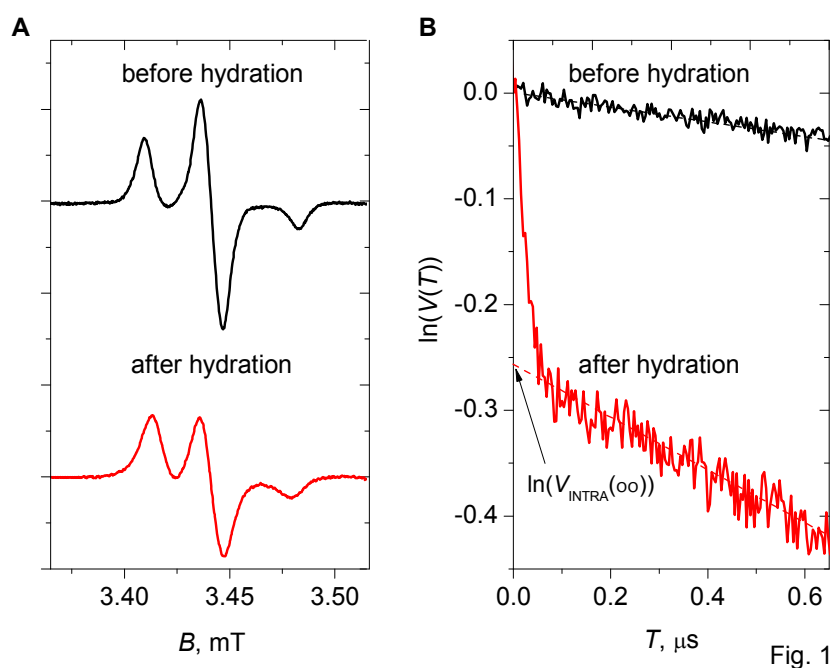

Fig. 1. (A) CW EPR spectra taken at 100 K for Alm16 in POPC membranes at the P/L ratio 1/400 before (top) and after (bottom) hydration. (B) Semi-logarithmic plot of the PELDOR time traces taken for the same samples (temperature: 80 K). Dashed lines show linear asymptotes and the intercept on vertical axis is assigned to the $\ln(V_{INTRA}(\infty))$ value.

Fig.1B presents the PELDOR time trace recorded for these two samples. Before hydration, the traces monotonically and slowly decay, whereas after hydration a fast initial decay at $T < 200$ ns takes place which is followed by a slower decay. The fast decay may be readily assigned to an increasing dipole⋯dipolar interaction between spin labels which

12

points to a peptide self-assembling into clusters (oligomers) in the membrane. The slow decay is assignable to interactions between clusters [see Eq. (1)].

Interestingly, the fast decay in the solid peptide/lipid film is not apparent even at the high P/L ratio~ 1/200 (ESI†, Fig. 2S), thus indicating that peptide oligomerization is exclusively induced by the membranes. Note also that slow decay for the hydrated sample is faster than the decay for the solid peptide/lipid film (see Fig. 1 B). This may be readily explained as a result of different spatial arrangements in the both cases: in the solid film the labels are randomly distributed in a 3-D space while after hydration the labels are arranged in a special way in 2-D space formed by bilayers, in the latter case the labels are located closer to each other.

4.2. The p_B calibration

In PELDOR experiments the p_B values were calibrated on the rigid biradical **BR** dissolved in a glassy methanol/ethanol mixture. The original PELDOR time traces for the frequency offsets ν_A-ν_B=±70 MHz are presented in Fig. 3S. The asymptotes fitting in Fig. 3S by straight lines resulted in $\ln(V_{INTRA}(\infty))$ values as intercepts on the vertical axis. These values were obtained for different pumping pulse amplitudes (data not shown). The p_B values were calculated for these amplitudes using Eq. (4). Then, the experimental $\ln(V_{INTRA}(\infty))$ values were plotted as a function of the calculated $\ln(1-p_B)$ values – see Fig. 2. The slope of the linear approximation for the data in Fig. 2 is expected to be determined by Eq. (7), in which the n value is taken for the biradical to be equal to2. This result, indeed observed in Fig. 2, justifies the correctness of the calculated p_B values.

For comparison, Fig. 2 reports also the data for Alm16 in POPC membranes at the P/L ratio 1/100 (full circles).Also these data display a linear dependence. However, here n=3.52,

thus clearly revealing that oligomers with $n > 2$ are formed. Note that the observed linearity

confirms that in our case the contribution of three-spin interactions is small.
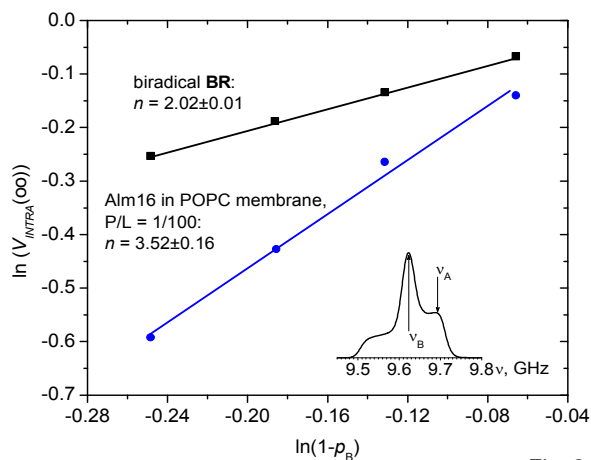

Fig. 2

Fig. 2. Logarithmic plot of the PELDOR signal asymptote $V_{INTRA}(\infty)$ on the $\ln(1 - p_B)$ values

for the biradical **BR** in glassy methanol/ethanol mixture (squares), and for Alm16 in POPC

membranes at the P/L ratio 1/100 (circles). The tangent of the line slope according to Eq. (7)

determines the n value, which is also indicated in the Figure. The positions of the pumping

and observation pulses in the EPR spectrum are indicated in the inset by arrows.

Temperature: 80 K.

4.3. EPR data for different peptide concentrations

Fig. 3A shows representative EPR spectra recorded for different P/L ratios in POPC

membranes. Note the linewidth broadening upon the P/L ratio increase. For Alm1 the

broadening is more pronounced than that for Alm16. This broadening may be assigned to the

magnetic dipole···dipolar interaction between spin labels. The spectral transformation upon

broadening may be qualitatively characterized by the ratio of the amplitudes of the central

and high-field components, d_1/d (Fig. 3 A). This ratio is plotted in Fig. 3B vs. the P/L ratio.

For comparison, the dotted horizontal line drawn at the d_1/d=0.39 value shows the data

obtained for Alm1 and Alm16 in a polar methanol/ethanol glass in which peptides may be assumed to be in the monomeric form. Then, the observed increase of d_1/d above this value can be ascribed to peptide self-assembling in the membranes.

The d_1/d value dependences in Fig. 3B for both Alm1 and Alm16 show a saturation-like behavior, with a fast increase below the P/L ratio 1/500, which is replaced by a slower growth at higher concentrations. Note that CW EPR spectra indicate self-assembling even at the lowest peptide concentrations studied.
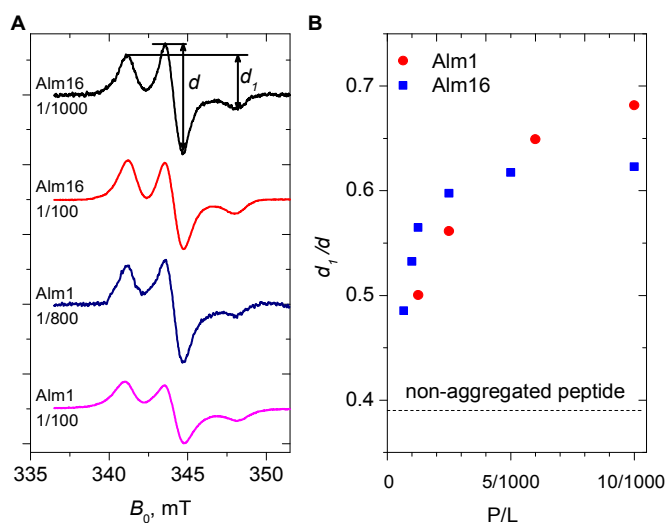

Fig. 3. (A) CW EPR spectra taken at 100 K for Alm16 and Alm1 at different P/L ratios. The d_1 and d values are shown by arrows. These values qualitatively describe spectral broadening. (B) The d_1/d dependence on the P/L ratio. The dotted line shows the lower limit obtained for a monomeric peptide in a methanol/ethanol glass.

It should be pointed out that some disagreement of the EPR lineshape shown in Fig. 3A for Alm1 at the P/L ratio 1/100 with previous data has been noted.[15] In our opinion, this observation could arise from an overestimated labeled material concentration. In the present

work, the concentration was additionally controlled by PELDOR measurements in a glassy

methanol/ethanol mixture, taking into account the exponential signal decay predicted by the

theory for monomeric spin labels[21] (Fig. 2S). (Our estimations have shown that the accuracy

of this PELDOR approach to measure spin concentration is about 20 %.)

4.4 PELDOR data for different peptide concentrations

Representative PELDOR time traces for samples with different P/L ratio values are

shown in Fig. 4. The dotted lines in Fig. 4 indicate the inter-cluster contribution to the signal

decay, $V_{INTER}(T)$. Their intercepts on the vertical axis determines the $\ln(V_{INTRA}(\infty))$ values. In

these measurements we found that these values are not influenced by the time delay τ when it
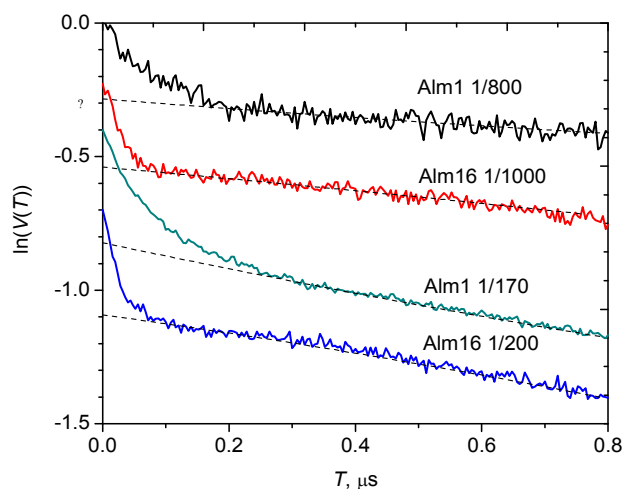
was varied between 0.4 and 0.8 μs.

Fig. 4. Semi-logarithmic plot of PELDOR time traces for Alm1 and Alm16 at different P/L

ratios. The data are shifted downward for convenience. The $V_{INTER}(T)$ time traces are shown

by dotted lines. Their intersections with the vertical axis determine the $\ln(V_{INTER}(\infty))$ values.

Temperature: 80 K.

As it follows from Eq. (7), the $V_{INTRA}(\infty)$ value directly provides the number n of peptides in an oligomer. The n values obtained for Alm1 and Alm16 are given in Fig. 5 along with the estimated experimental error bars. Data in Fig. 5 show a saturation-like dependence, with a kink at the P/L ratio 1/500, which is similar to that in the CW EPR data (Fig. 3B).

Fig. 5 shows that at small P/L ratios for both Alm1 and Alm16 the n value is close to 2. Therefore, the peptide molecules are self-assembled even at small concentrations, at least into dimers. As the P/L ratio approaches 1/100, the n value becomes close to 4, which is in agreement with previous PELDOR data for Alm1 and Alm16 in ePC membranes.[7]

Note that in the aforementioned experiments the 3-pulse PELDOR is preferable, as compared with the commonly employed 4-pulse PELDOR because $V_{INTRA}(T)$ in the 4-pulse PELDOR is noticeably lower than that in the 3-pulse PELDOR (see Fig. 4S in ESI† and also the discussion in an earlier work).[39] To increase $V_{INTRA}(T)$ in the 4-pulse PELDOR, one should use shorter pulse length.[29-31] However, in our case this shortening may violate the condition $p_B(n-1) < 1$ which would result in an underestimated n value.
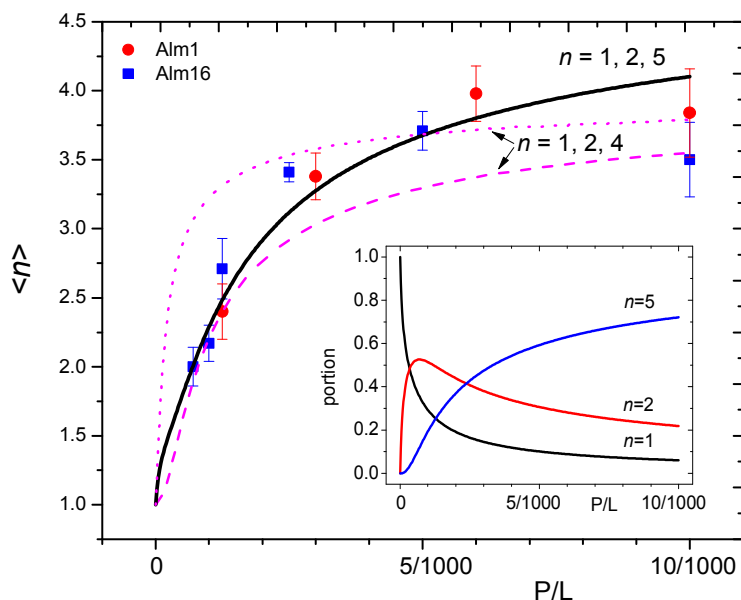
Fig. 5. The mean number of molecules in a cluster for Alm1 (full circles) and Alm16 (full squares), obtained using Eq. (7) for different P/L ratios in the POPC membranes. Simulation for the model of equilibrium between monomers, dimers, and tetramers is given by the dashed and dotted lines (fitting respectively the beginning and the asymptote of the dependence). The solid curve is the simulation for the model of equilibrium between monomers, dimers and pentamers, with fitting parameters $p_2 = 3 \cdot 10^3$ (P/L)$^{-1}$ and $p_5 = 2 \cdot 10^6$ (P/L)$^{-2}$ (see text). The inset shows the concentration dependence for the portions of monomers, dimers, and pentamers.

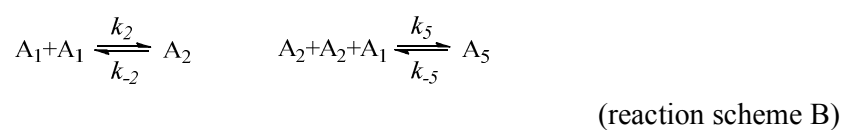## 4.5. Kinetic model of peptide assembling

As mentioned above, different models were proposed in the literature for the Alm self-assembling in biological membranes, suggesting formation of oligomers with number of Alm molecules varying from 2 to 8. We consider here only formation of dimers, tetramers[7] and pentamers.[8] To describe the whole concentration dependence presented in Fig. 5, it is

necessary to consider an equilibrium between oligomers of different order. Tetramers (A_4) might be formed *via* subsequent self-assembling of monomers (A_1) and dimers (A_2):

$$A_1 + A_1 \underset{k_{-2}}{\overset{k_2}{\rightleftharpoons}} A_2 \qquad A_2 + A_2 \underset{k_{-4}}{\overset{k_4}{\rightleftharpoons}} A_4$$
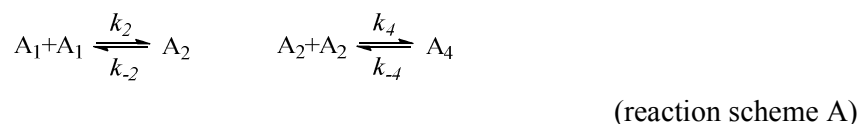
(reaction scheme A)

For pentamer formation, we employed here a simple kinetic gross-scheme including only monomers, dimers, and pentamers (A_5):

$$A_1 + A_1 \underset{k_{-2}}{\overset{k_2}{\rightleftharpoons}} A_2 \qquad A_2 + A_2 + A_1 \underset{k_{-5}}{\overset{k_5}{\rightleftharpoons}} A_5$$

(reaction scheme B)

The three-molecular reaction may occur *via* two stages, with only two molecules associating in the intermediate steps.

Denoting the reaction constant ratios as

$$p_2 = \frac{k_2}{k_{-2}}, \quad p_4 = \frac{k_4}{k_{-4}} \quad p_5 = \frac{k_5}{k_{-5}}, \tag{10}$$

and a_1, a_2, a_4, a_5 as the corresponding concentrations, at the equilibrium we obtain

$$a_2 = p_2 a_1^2, \quad a_4 = p_4 a_2^2 = p_4 p_2^2 a_1^4, \quad a_5 = p_5 a_2^2 a_1 = p_5 p_2^2 a_1^5 \tag{11}$$

Having in mind that the total concentration of peptides, a, remains constant, the concentrations obey the relation

$$a_1 + 2a_2 + 4a_4 = a$$

for the reaction scheme (A) and

$$a_1 + 2a_2 + 5a_5 = a$$

for the reaction scheme (B). Then, we immediately obtain that a_1 obeys the equations

$$a_1 + 2p_2a_1^2 + 4p_2^2p_4a_1^4 = a$$
$$a_1 + 2p_2a_1^2 + 5p_2^2p_5a_1^5 = a \text{ '}$$
$$(12)$$

in the former and latter cases, respectively. These equations can be solved numerically for different values of the parameters p_2, p_4, and p_5, and for different concentrations a. With the a_1 value obtained, for the measured mean number n we then have:

$$< n >= \frac{1}{a}(a_1 + 4a_2 + 16a_4) \qquad (13 \text{ A})$$

$$< n >= \frac{1}{a}(a_1 + 4a_2 + 25a_5), \qquad (13 \text{ B})$$

in the former and latter cases, respectively.

The dashed and dotted lines show results of the calculations from Eq. (13 A). In this case the data can be fitted either for the initial part of the dependence (dashed line) or for the dependence asymptote (dotted line), but not for the whole experimental data point dependence. The solid line in Fig. 5 presents the calculated [Eq. (13 B)] dependence of n taken as a function of concentration a. We notice a fairly good agreement between experiments and calculations. The fitting parameters p_2 and p_5 determining this dependence are given in caption to Fig. 5 in $(P/L)^{-1}$ and $(P/L)^{-2}$ units, respectively.

The inset in Fig. 5 shows how monomers, dimers, and pentamers, calculated for the reaction scheme (B), change upon varying the total peptide concentration. It is clear that already at the very small P/L ratio 1/1500 peptides are assembling into dimers.

Obviously, the experimental data in Fig. 5 may be fitted with other models of oligomerization which may include formation of trimers, tetramers, hexamers, *etc*. One definite restriction only can be imposed from the above analysis, namely that oligomers with $n \geq 5$ indeed are formed under our experimental conditions.

4.6. ^{2}H ESEEM data for different peptide concentrations

For the membrane hydrated by deuterated water, the amplitude of ^{2}H ESEEM provides information on the closeness of the label to the membrane surface.[25,40,41] In Fig. 6 A, representative data on normalized ESEEM time traces are given for Alm1 and Alm16 (P/L ratio 1/200). For comparison, the analogous data for the spin-labeled lipid Tempo-PC and the spin-labeled stearic acid, 5-DSA (see Experimental) in the membranes are also shown. In the former case, the ESEEM amplitude corresponds to the water amount on the membrane surface, in the latter case to that near the 5th carbon atom position in the acyl chain of the embedded stearic acid (and probably, of the POPC lipid) in the membranes.
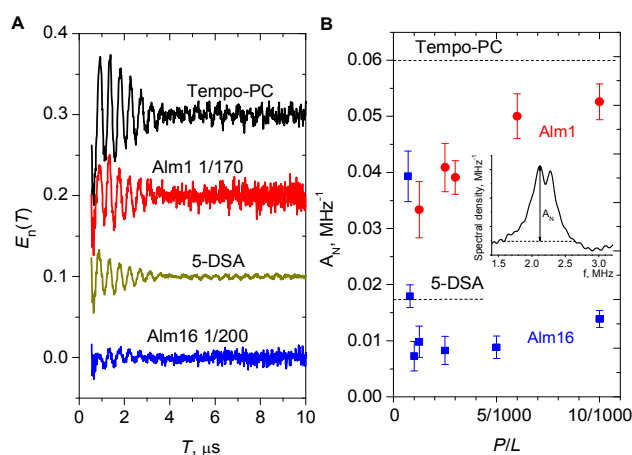

Fig. 6

Fig. 6. (A) Representative data for the normalized time-domain ESEEM time traces, $E_n(T)$, for Alm1 and Alm16 at different P/L ratios, along with analogous data for spin-labeled lipids Tempo-PC and 5-DSA (1 mol. % in both cases). (B) The amplitudes, A_N, (see inset for its determination) of the ESEEM frequency spectra *vs.* the P/L ratio. The dashed lines show the A_N values for Tempo-PC and 5-DSA.

Fig. 6B shows the ESEEM amplitude A_N plotted for Alm1 and Alm16 as a function of the P/L ratio. First, for Alm16 the A_N value abruptly drops when the P/L ratio is increased from its smallest value 1/1500. (The amplitude of the initial point at the P/L ratio 1/1500 shown in Fig. 6B is an average value obtained in several measurements with different samples). These data may be readily interpreted as an evidence that the peptide orientation in the membranes changes sharply from the in-plane to the transmembrane with the P/L ratio attaining the 1/1000 value.

Also, the A_N value for Alm1 at a P/L ratio > 1/1000 is much stronger than that for Alm16, which means that the spin label attached to the 1st amino acid position in the peptide sequence is located closer to the membrane surface than that at the 16th position. Note that the similar conclusions on the peptide localization in membrane can be drawn from the A_{ZZ} splitting observed in the CW spectra[42,43] (see ESI†, Fig. 5S).

The result on peptide reorientation is to be compared with the above PELDOR data on peptide oligomerization. In both cases, reorientation and dimer formation occur at nearly the same P/L ratio (~ 1/1000). So one may suggest that reorientation and dimer formation are concurrent processes. The both data sets, ESEEM in Fig. 6 B and PELDOR in Fig. 5, demonstrate very sharp concentration dependence at small concentrations (and the CW EPR data in Fig. 3 B as well), so it is difficult to conclude whether the dimer formation precedes the peptide reorientation or these two processes occur simultaneously. (One more possibility – that peptide reorientation precedes dimerization – may be ruled out because a driving force for this process is unclear.)

4.7. Distances between spin labels in the oligomers from PELDOR data analysis

The representative $V_{norm}(T)$ PELDOR data [see Eq. (5)] are shown in Fig. 7 A. Their Fourier transforms (Pake patterns) are given in Fig. 7 B. As the P/L ratio increases, the Pake pattern becomes remarkably broader (with high-frequency wings appearing).
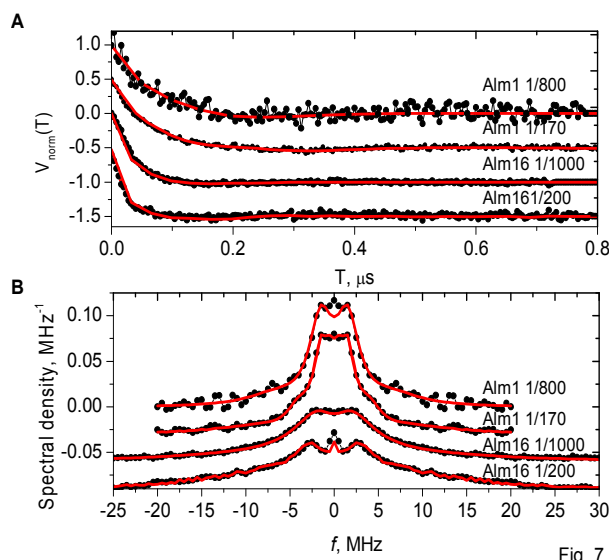

Fig. 7. (A) Normalized experimental (dots) PELDOR time traces for Alm1 and Alm16, taken at two different P/L ratios, and their simulations (solid lines). (B) The same traces in the frequency domain. See text for other details.

Here, we restrict our analysis of PELDOR data in Fig. 7 by the pairwise model of PELDOR signal formation [Eqs. (2) – (5)]. This approach is applicable under our experimental conditions, namely with $p_B \sim 0.22$, because the probability to excite high-order harmonics (sum or difference of two dipolar frequencies)[29-31] is not expected to be large. However, it is necessary to keep in mind that higher-order harmonics may create ghost peaks in the distance distribution spectrum (at distances shorter or longer than those where real peaks are located).[29-31]

Physical Chemistry Chemical Physics Accepted Manuscript

It should be noted that a reliable distance region between spin probes obtained from PELDOR experiments depends on two factors: the lower-distance boundary is restricted by the pumping pulse length,[44,45] while the upper-boundary is determined by the experimental PELDOR decay.[45] We estimated that under our experimental conditions the reliable distance region is 1.6-3.7 nm.

Simulation of the Pake pattern in the frequency domain was performed by a multi-Gaussian fully-random Monte Carlo algorithm.[34] Results are given in Fig. 7 both in the time and frequency domains. The rate of convergence of the Monte Carlo process is illustrated in Fig. 6S. To attain a fairly good description of the experimental data, in all cases it was enough to employ only three Gaussians with varying width and position. In Figs. 7S and 8S we also provide comparison with the results of traditional Tikhonov regularization approach.[31] (Some difference between the results of two approaches is seen in Fig. 7S; it may be ascribed to the ill-posed nature of the problem, however this difference is not dramatic.)

The best-fit distance distributions $P(r)$ functions found in this approach for Alm1 and Alm16 are shown in Fig. 8. Note that the peaks at the shortest distances (1.5 nm) are not reliable because they may contain contributions from three-spin interactions (see above). For Alm1, two almost distinct groups are observed at 1.8-2.2 nm and 2.8-3.5 nm (the peak position depends on peptide concentration), while for Alm16 an overlapping sum of peaks at 1.5-2.4 nm is seen. As the P/L ratio increases for both Alm1 and Alm16, the lines become narrower and slightly shifted to longer distances.

The simulated $P(r)$ distributions were obtained under the assumption that the orientation selectivity, known from the PELDOR experiment,[29-31] would be absent. This assumption is justified both by the flexibility of the Alm molecules (mixed α-/3_{10}-helices in the membranes are assumed)[7,46] and by the loose structures of the oligomers (Fig. 8). The

freedom in the peptide orientation of the oligomers broadens the interspin distances and smoothens the orientation selectivity effects.[47]
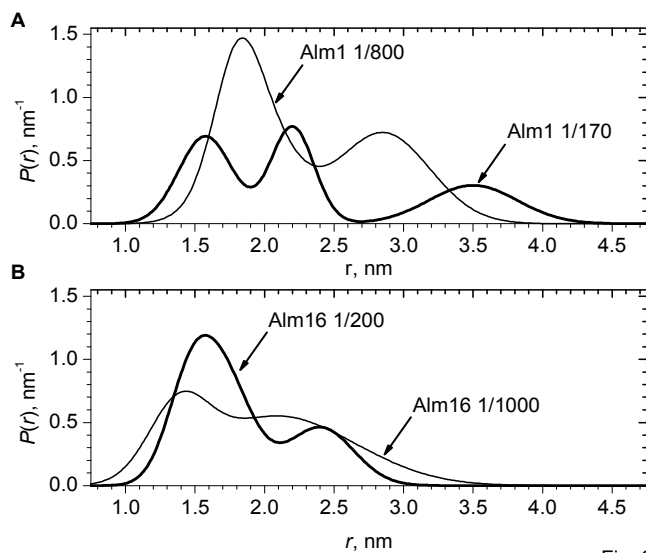

Fig. 8

Fig. 8. Distance distribution functions: (A) for Alm1 at the P/L ratios 1/800 (thin lines) and 1/170 (bold lines); (B) for Alm16 at the P/L ratios 1/1000 (thin lines) and 1/200 (bold lines). The peaks around 1.5 nm may contain ghost peaks arisen from three-spin interactions.

5. Discussion

As it was stated above, the experimental data obtained may be fitted with oligomerization of different degree: formation of dimers, trimers, tetramers, pentamers, hexamers. However one may suggest a definite model which would be in agreement with all the PELDOR and ESEEM data obtained and the data available in the literature,[16,17] and which would be useful for further discussion and future development. Such a model is presented in Fig. 9, where, like it was proposed above, the dimer and pentamer formation is assumed.

The peptide molecules are assumed in Fig. 9 to have a helix kink at Pro 14 position,[48] that minimize the mismatch conditions. The dimer structure resembles a hybrid between a

"funnel" or "sandglass" shape.[17] The label positions indicated explain the difference for interspin distances between two 1st positions and two 16th positions in the dimer (the distance is larger for Alm1) and the difference for ESEEM amplitudes in D_2O-hydrated membranes (Alm1 is closer to the membrane surface). The different water-accessibility found in ESEEM (see Fig. 6) also may be caused by different spin-probe location – the 1st position is in the outer side of the helix that is close to the surrounding water, while the 16th position is in the core of channel. According to the previous CW EPR study,[15] the shortest distances between peptides in the dimer are observed in the region between the 7th and 9th residues (see Fig. 9 A) that correlates with published data.[8] The "isthmus" position near the 7th and 9th residues corresponds to hydrogen-bond network between amino acids at 7th position.[17] Therefore, Alm dimers likely adopt a "sandglass" shape (Fig. 9A). This shape would also explain why the $P(r)$ distribution for the dimers contains shorter and more resolved distances for Alm16 as compared with those for Alm1 (Fig. 8).

The bifurcation of $P(r)$ into two peaks at increasing P/L ratio (Fig. 8) is readily explained by the pentamer structure: while there is only one partner in a dimers (shown as N1 in Fig. 9B), in a pentamer (Fig. 9C) there are two partners – the nearest and remote neighbors (N1 and N2, respectively). The narrowing of $P(r)$ observed with increasing the P/L ratio (Fig. 8) may be also related with the oligomerization process: in dimers the helices possess some freedom in their mutual motion, while in pentamers this freedom is lost.

The simplest oligomer model is an equilateral "flower-like" structure, as it shown in Fig. 9C. For degree of oligomerization $n > 3$, each peptide molecule has here a nearest neighbor N1 with intermolecular distance r_1 and a remote neighbor N2 with intermolecular distance r_2. Simple geometric consideration shows that the ratio r_2/r_1 is expected to be 1.4, 1.6 and the mixture of 1.7 and 2.0 for tetramer, pentamer and hexamer structures, correspondingly. Data in Fig. 8 provide that $r_2/r_1 \sim 1.59$ for Alm1 (at P/L = 1/170) and $r_2/r_1 \sim 1.54$ for Alm16 (at

P/L = 1/200), that is in favour of the pentamer structure. However, the broad peaks for remote

neighbours in Fig. 8 allows suppose an admixture of higher oligomers as well. Note however

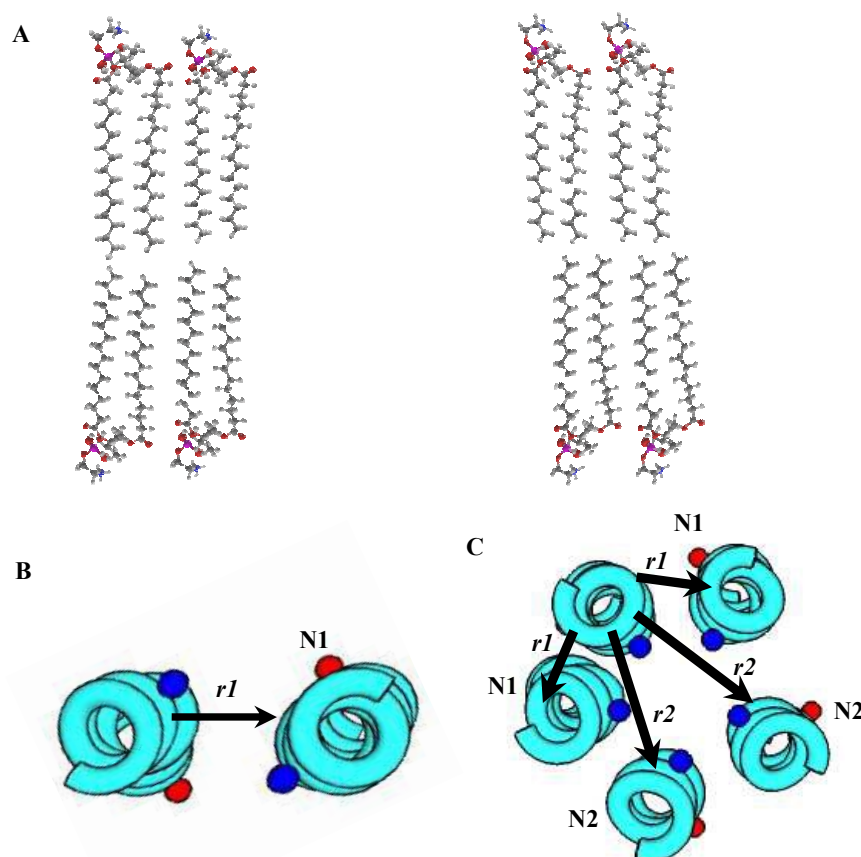that we assume here parallel helix alignment, but the antiparallel one is also possible.[17]

Fig. 9

Fig. 9. The suggested model of Alm oligomerization and localization in the membrane.

(A) Side view: dimers of the peptide helices and the surrounding lipids. The spin labels at the

Aib[1] and Aib[16] positions are marked as red and blue full circles, respectively. The kink seen

in the helix structure is located near the Pro[14] position.[48] (B) Top view of the dimers. The

neighbor of type N1 is marked by an arrow. (C). Top view of the pentamers. The neighbors of the N1 and N2 types are marked. The distances r_1 and r_2 for space separation between peptides are shown by arrows (see text).

The previous models of Alm oligomerization in the ePC[7] and POPC[8,15] membranes suggested the transmembrane peptide location for a P/L ratio > 1/200 (the lowest P/L ratio value employed in these studies), with the peptide N-terminus closer to the membrane surface (in agreement with the results reported here). Also, there was evidence from the CW EPR data that in POPC membranes, even at the P/L ratio 1/100, the Alm molecules would aggregates.[15] PELDOR and ESEEM data obtained for ePC membranes[7] were explained within a tetramer "pen-knife" model: two peptides have a transmembrane alignment, while the other two peptide helices are tilted. Such localization gives a distance distribution for Alm16 (P/L ratio 1/70) with a maximum at 2.3 nm, which is in agreement with data reported here for POPC membranes. For Alm1 in ePC membranes (P/L ratio 1/70) two peaks were seen (a broad peak extending from ~ 2.0 to 3.5 nm and a second broad peak centered at 5.2 nm. In the POPC membranes studied here for Alm16 at the P/L ratio 1/200 we observed two overlapping peaks located between 2 and 4 nm (Fig. 8B), which is again in agreement with the literature data.[7] The low-amplitude, broad peak found for longer distances[7] was not reproduced in our studies. However, the experimental data in Fig. 7 are simulated fairly well in the absence of this broad distribution.

The NMR data on Alm in POPC membrane[8] showed the transition from dimers to pentamers with the P/L ratio increasing from 1/30 to 1/13. This result is in disagreement with our measurements (see inset in Fig. 5) where this transition is observed at much lower P/L ratio. We ascribe this discrepancy to two factors: (i) The different sensitivity of the methods –

the NMR distance measurement sensitivity is restricted to ~ 1.5 nm, whereas for PELDOR only distance values larger than 1.5 nm are detected reliably. Therefore, some dimers seen in the NMR experiments may belong to pentamers. (ii) The slightly different amino acid sequences employed in the two studies: the ^{19}F-substituted analog in NMR[8] and the spin-label-substituted analog studied by EPR in this work.

The shorter interspin distances observed at the P/L ratio 1/100 for Alm1 by CW EPR measurements[15] and at the P/L ratio 1/13 for Alm9 (spin labeled at the 9th position),[8] correlate with our proposed "sandglass" model, in which the 8th residue is located exactly near the sandglass isthmus.

Finally, we would like to also mention the literature data on the Alm effects which are noticeable in lipid membranes even at low peptide concentration. The circular dichroic and fluorescent data on Alm in phospholipid membranes[49] show that Alm oligomerization starts at P/L ratio ~1/1000. Small-angle neutron scattering shows that Alm enriches the outer leaflet of the bilayer with the negatively charged lipids, thus creating an asymmetric distribution of lipids: the enrichment occurs at a P/L ratio ~1/1000 – 1/200 and it disrupts a lateral inhomogeneity seen in lipid/cholesterol vesicles (P/L ratio of 1/200).[50] Pulsed EPR of spin labels shows that Alm can capture fatty acids present in the membranes, even at a P/L ratio of 1/500.[51] These destabilizing effects on the membranes were taken to suggest[50,51] mechanisms of peptide antimicrobial action alternative to the standard models involving pore formation.

6. Conclusions

Our study of spin-labeled Alm analogs in POPC bilayers at P/L ratios varying between 1/1500 and 1/100, and employing different EPR techniques (CW EPR, PELDOR and ESEEM), demonstrated that self-assembling of Alm molecules starts with dimer formation, which occurs at the smallest P/L ratio used. Concurrently with dimer formation, peptides

change their orientation in the bilayer from the in-plane to the trans-membrane. As the P/L ratio increases, peptides assemble into higher oligomers (channels) which may include pentamers and higher oligomers. The dimers observed at lower peptide concentration may be precursor states for the channel formation.

The inter-label distance distribution becomes more resolved with increasing the P/L ratio, thus suggesting that the higher oligomers possess a more defined structure.

In the case of an equilibrium between oligomers of different order, to determine the number of molecules forming an oligomer, a correct PELDOR data analysis requires a detailed investigation of the peptide concentration dependence. Otherwise, this number may be underestimated.

Finally, we believe that the EPR techniques exploited in this work to study peptide aggregates (channels) in membranes can be productively extended to related research topics, such as the channel-forming inclusion compounds.[52,53]

Physical Chemistry Chemical Physics

References

1. C. Toniolo, H. Brückner, H., Eds, *Peptaibiotics: Fungal Peptides Containing α-Dialkyl α-Amino Acids,* Verlag Helvetica Chimica Acta, Zurich and Wiley-VCH, Weinheim, 2009.

2. H. Duclohier, *Curr. Pharm. Design, 2010,* **16**, 3212-3223.

3. G. Bocchinfuso, A. Palleschi, B. Orioni, G. Grande, F. Formaggio, C. Toniolo, Y. Park, K.-S. Hahm, L. Stella, *J. Pept. Sci.*, *2009*, **15**, 550-558.

4. N. K. N. Neumann, N. Stoppacher, S. Zeilinger, T. Degenkolb, H. Brückner, R. Schuhmacher, *Chem. Biodivers.*, *2015,* **12**, 743-751.

5. M. S. P. Sansom, *Eur.Biophys. J.*, *1993*, **22**, 105-124.

6. H. Vogel, *Biochemistry*, *1987*, **26**, 4562-4572.

7. A. D. Milov, R. I. Samoilova, Yu. D. Tsvetkov, M. De Zotti, F. Formaggio, C. Toniolo, J.-W. Handgraaf, J. Raap, *Biophys. J.*, *2009*, **96**, 3197-3209.

8. E. S. Salnikov, J. Raya, M. De Zotti, E. Zaitseva, C. Peggion, G. Ballano, C. Toniolo, J. Raap, B. Bechinger, *Biophys. J.,2016*, **111**, 2450-2459.

9. B. Bechinger, *J. Pept. Sci.*, *2015*, **21**, 346-355.

10. H. W. Huang, Y. Wu., *Biophys. J.*, *1991*, **60**, 1079–1087.

11. K. He, S. Ludtke, W. Heller, H. Huang, *Biophys.J.*, *1996*, **71**, 2669-2679.

12. L. Stella, M. Burattini, C. Mazzuca, A. Palleschi, M. Venanzi, I. Coin, C. Peggion, C. Toniolo, B. Pispisa, *Chem. Biodivers.*, *2007*, **4**, 1299-1312.

13. M. Barranger-Mathys, D. S. Cafiso, *Biophys. J.*, *1994*, **67**, 172-176.

14. B. Bechinger, D. A. Skladnev, A. Ogrel, X. Li, E. V. Rogozhkina, T. V. Ovchinnikova, J. D. J. O'Neil, J. Raap, *Biochemistry*, *2001*, **40**, 9428-9437.

15. E. S. Salnikov, M. De Zotti, F. Formaggio, X. Li, C. Toniolo, J. D. J. O'Neil, J. Raap, S. A. Dzuba, B. Bechinger, *J. Phys. Chem. B*, *2009*, **113**, 3034-3042.

16. D. P. Tieleman, B. Hess, M. S. P. Sansom, *Biophys. J.*, *2002*, **83**, 2393-2407.

Physical Chemistry Chemical Physics Accepted Manuscript

17. A. Rahaman, T. Lazaridis, *Biochim. Biophys. Acta*, *2014*, **1838**, 1440-1447.

18. H. W. Huang, *Biochim. Biophys. Acta*, *2006*, **1758**, 1292–1302.

19. M. Bortolus, M. De Zotti, F. Formaggio, A. L. Maniero, *Biochim. Biophys. Acta (Biomembranes)*, *2013,* **1828**, 2620-2627.

20. A. D. Milov, K. M. Salikhov, M. D. Shirov, *Fizika Tverd. Tela, 1981*, **23**, 975-982.

21. A. D. Milov, A. G. Maryasov, Yu. D. Tsvetkov, *Appl. Magn. Reson.*, *1998*, **15,** 107-143.

22. G. Jeschke, Y. Polyhach, *Phys. Chem. Chem. Phys. 2007*, 9, 1895-1910.

23. O. Schiemann, T. F. Prisner, *Quart. Rev. Biphys. 2007*, 40, 1-53.

24. S. A. Dzuba, J. Raap, *Chem. Biodivers. 2013*, **10**, 864-875.

25. S. A. Dzuba, D. Marsh, *ESEEM of Spin Labels to Study Intermolecular Interactions, Molecular Assembly and Conformation.* In: *A Specialist Periodic Report, Electron Paramagnetic Resonance*, 2015, **24**, 102–121. Eds. C. Gilbert, V. Chechik, D.M. Murphy, RSC Publishing.

26. A. D. Milov, Y. D. Tsvetkov, J. Raap, M. De Zotti, F. Formaggio, C. Toniolo, *Biopolymers*, *2016*, **106**, 6-24.

27. K. M. Salikhov, I. T. Khairuzhdinov, R. B. Zaripov, *Appl. Magn. Reson., 2014*, **45**, 573-619.

28. A. D. Milov, Yu. D. Tsvetkov, M. De Zotti, C. Prinzivalli, B. Biondi, F. Formaggio, C. Toniolo, M. Gobbo**,** *J. Struct. Chem.*, *2013*, **54**, 73-85.

29. T. von Hagens, Y. Polyhach, M. Sajid, A. Godt, G. Jeschke, *Phys. Chem. Chem. Phys.*, *2013*,**15**, 5854-5866.

30. G. Jeschke, M. Sajid, M. Schulte, A. Godt, *Phys. Chem. Chem. Phys.*, *2009*,**11**, 6580-6591.

31. G. Jeschke, V. Chechik, P. Ionita, A. Godt, H. Zimmermann, J. Banham, C. R. Timmel, D. Hilger, H. Jung, *Appl. Magn. Reson.*, *2006*, **30**, 473-498.

32. S. A.Dzuba, *J. Magn. Reson. 2016*, **269**, 113-119.

33. P. G. Fajer, M. Gyimesi, A. Málnási-Csizmadia, C. R. Bagshaw, K. I. Sen, L. Song, *J. Phys.: Condens. Matter, 2007,* **19**, 285208.

34. A. G. Matveeva, Yu. V. Yushkova, S. V. Morozov, I. A. Grygor'ev, S. A. Dzuba, *Z. Phys. Chem.*, *2017*, **231**, 671-688.

35. B. E. Bode, D. Margraf, J. Plackmeyer, G. Dürner, T. F. Prisner, O. Schiemann, *J. Am. Chem. Soc.*,*2007*, **129**, 6736-6745.

36. C. Peggion, M. Jost, C. Baldini, F. Formaggio, C. Toniolo, *Chem. Biodivers., 2007*, **4**, 1183-1199.

37. C. Peggion, I. Coin, C. Toniolo, *Biopolym., 2004*, **76**, 485–493.

38. A. Akbarzadeh, R. Rezaei-Sadabady, S. Davaran, S. W. Joo, N. Zarghami, Y. Hanifehpour, M. Samiei, M. Kouhi, K. Nejati-Koshki, *Nanoscale Res. Lett.*, *2013*, **8**, 102.

39. A. D. Milov, Yu. A. Grishin, S. A. Dzuba, Yu. D. Tsvetkov, *Appl. Magn. Reson.*, *2011*, **41**, 59-67.

40. D. A. Erilov, R. Bartucci,R. Guzzi, A. A. Shubin, A. G. Maryasov, D. Marsh, S. A. Dzuba, L. Sportelli, *J. Phys. Chem. B*, *2005,* **109**, 12003-12013.

41. A. D. Milov, R. I. Samoilova, A. A.Shubin, Yu. A. Grishin, S.A. Dzuba, *Appl. Magn. Reson.*,*2008*,**35**, 73-94.

42. H. J. Steinhoff, M. Pfeiffer, T. Rink, O. Burlon, M. Kurz, J. Riesle, E. Heuberger, K. Gerwert, D. Oesterhelt, *Biophys. J.*,*1999*, **76**, 2702-2710.

43. L. Urban, H. J. Steinhoff, *Mol. Phys.*,*2013*, **111**, 2873-2881.

44. A.D. Milov, B.D. Naumov, Yu.D. Tsvetkov, *Appl. Magn. Reson., 2004, 26,* 587-599.

45. G. Jeschke, *Annu. Rev. Phys. Chem., 2012,* **63,** 419–446.

46. E. S. Salnikov, H. Friedrich, X. Li, P. Bertani, S. Reissmann, C. Hertwerk, J. D. J. O'Neil, J. Raap, B. Bechinger, *Biophys. J. 2009*, **96**, 86-100.

47. G. Jeschke, A. Koch, U. Jonas, A. Godt, *J. Magn. Reson.*, *2002*, **155**, 72-82.

48. J. Dittmer, L. Thøgersen, J. Underhaug, K. Bertelsen, T. Vosegaard, J. M. Pedersen, B. Schiøtt, E. Tajkhorshid, T. Skrydstrup, N. C. Nielsen, *J. Phys. Chem. B*, *2009*, **113**, 6928-6937.

49. V. Rizzo, S. Stankowski, G. Schwarz, *Biochem. 1987*, **26**, 2751–2759.

50. S. Qian, W. T. Heller, *J. Phys. Chem. B*, *2011*, **115**, 9831-9837.

51. E.F. Afanasyeva, V. N. Syryamina, S. A. Dzuba, *J. Chem. Phys.*, *2017*, **146**, 011103.

52. H. Kobayashi, Y. Furuhashi, H. Nakagawa, T. Asaji, *Magn. Reson. Chem., 2016,* **54**, 641-649.

53. A. Barbon, A. Zoleo, M. Brustolon, A. Comotti, P. Sozzani, *Inorg. Chim. Acta*, *2008*, **361**, 4122–4128.

Physical Chemistry Chemical Physics Accepted Manuscript